A Unified Analysis of Security-Constrained OPF Formulations Considering Uncertainty, Risk, and Controllability in Single and Multi-area Systems

Maria Vrakopoulou, Spyros Chatzivasileiadis, Emil Iggland, Markus Imhof, Thilo Krause, Olli Mäkelä, Johanna L. Mathieu, Line Roald, Roger Wiget, and Göran Andersson

EEH - Power Systems Laboratory, ETH Zurich, Physikstrasse 3, 8092 Zurich, Switzerland
E-mail: {vrakopoulou, andersson}@eeh.ee.ethz.ch

Abstract

This paper presents a variety of different Security Constrained Optimal Power Flow formulations addressing four power system operation and planning problems: (a) forecast uncertainty of Renewable Energy Sources (RES) in-feed and load, (b) security criteria based on contingency risk, (c) corrective control offered through High Voltage Direct Current (HVDC) lines and flexible demand, (d) operation of multi-area systems with limited data exchange. A comprehensive probabilistic Security Constrained Optimal Power Flow (SCOPF) framework based on scenario-based methodologies is presented. This approach provides a-priori guarantees regarding the probability of the constraint satisfaction. In this paper, we show how HVDC lines, flexible demand, and novel risk-based operational paradigms can be used to handle outage uncertainty and the fluctuating in-feed from RES. Our analysis is extended by introducing a distributed probabilistic SCOPF algorithm for multi-area systems involving different levels of data exchange. The applicability of the methods is demonstrated on the three-area Reliability Test System (RTS-96). Results are compared based on operating costs and maximum wind power penetration.

I. Introduction

Fossil resource depletion, climate change, market liberalisation, and technological progress are among the major drivers strongly influencing current paradigms for power system planning and operation. In particular, there is a growing need to accommodate the increasing in-feed from RES in a secure and economically efficient manner. Additionally, European energy policy aims to establish a pan-European electricity market. Moreover, the demand side is undergoing significant changes. For example, the widespread deployment of smart metering infrastructure together with a possible increase in electric mobility will allow for increased demand side participation.

The above mentioned developments pose both threats and opportunities for power system operation and control. Increased integration of RES with fluctuating power in-feed calls for probabilistic operational approaches taking into account potentially large variations in real-time power production. Due to the increased level of uncertainty, new security criteria – beyond the classical N-1 criterion – need to be considered to allow us to quantify contingency risks more effectively. Related adverse effects may be countered by controllable elements that could act not only preventively, but also correctively. Such controllable elements comprise e.g. generators, loads and HVDC lines (either as point-to-point links or as HVDC grids). The controllability of these elements could (a) maximize the RES infeed, (b) reduce operating costs, and (c) defer investments in new transmission lines.

Our paper discusses these options as follows: First, we quantify how N-1 security as well as uncertainty increase operational costs. In a second step, we demonstrate how this cost rise can be countered by risk-based security concepts in conjunction with novel control schemes taking advantage of the controllability of generators, loads and HVDC technology. We also show how control schemes can be used to maximize the level of RES in-feed. For that purpose we rely on novel SCOPF formulations to handle uncertainties in an improved manner. Our analysis is not restricted to single-area systems but also discusses the operation of multi-area systems involving different Transmission System Operators (TSOs) and different levels of data exchange.

The contribution of this paper is threefold. First, a comprehensive probabilistic SCOPF framework based on scenario-based methodologies is presented, where different levels of uncertainty, controllability, and contingency risk are incorporated in one algorithm. The scenario-based methodologies provide a-priori guarantees regarding the probability of the constraint satisfaction while requiring no assumptions on the probability distribution of the uncertain variables. Second, a distributed probabilistic SCOPF algorithm for multi-area systems is presented. Third, the performance of the different SCOPF formulations are compared in several case studies on the three-area Reliability Test System (RTS)-96 system. Performance criteria are the operating costs and the maximum wind power penetration.

The remainder of the paper is organized as follows:

Section II presents a generic formulation of the SCOPF problem introducing briefly the general idea behind the SCOPF together with the basal optimization problem.

Section III considers different levels of uncertainty. First, a probabilistic SCOPF is proposed where wind and load forecast errors are taken into account. All line and generator outages are assumed as critical contingencies, and, in this first stage, no corrective control actions are allowed. The method is extended

978-1-4799-0199-9/13/ $31.00

by introducing a risk-based approach as a security criterion, where the contingencies are ranked based on their probability of occurrence and the severity of the post-contingency state.

Section IV focuses first on preventive and corrective control actions by 1) flexible but uncertain loads and 2) point-to-point HVDC links and meshed HVDC grids. In addition to actively controlling the power flow, HVDC lines based on the Voltage Source Converter (VSC) technology have the ability to react fast in case of a contingency and relieve possible line overloading or avoid large voltage deviations.

Section V exemplifies the previously developed theoretical concepts in a case study, relying on a slightly modified version of the three area RTS-96 system. Operating costs and maximum wind penetration are compared for different levels of uncertainty and controllability.

Section VI presents applications of a probabilistic SCOPF in multi-area systems and compares operation schemes with different levels of information exchange between the areas.

Section VII discusses the limitations of a steady-state SCOPF in terms of handling transient phenomena, which may take place after a contingency or during corrective control actions. Although such phenomena could lead to instability, dynamic control actions offered through, for example, HVDC lines could help mitigate their effect on the system.

Section VIII concludes the paper.

II. Generic SCOPF Formulation

The SCOPF extends the Optimal Power Flow (OPF) problem by incorporating additional constraints resulting from the operation of the system under a set of possible contingencies [1]. First formulations, for example in [2], focused on preventive control actions. The objective was to identify the optimal setpoints for the control variables in the pre-contingency state so that the power system remains secure in the event of all considered contingencies. Subsequent developments included the identification of corrective control actions, which would be applied in the occurrence of a contingency [3].

One of the major SCOPF challenges is the large problem size. Typically, the SCOPF is a non-linear, non-convex, large-scale optimization problem with both continuous and discrete variables [2]. In this paper, we consider only continuous variables. In order to jointly handle contingencies, uncertainty, and corrective control actions, we assume linearized equations for both the pre-contingency and the post-contingency states in the form of a DC SCOPF. Eq. (1)-(3) present a generic formulation of the SCOPF problem as it will be used throughout the paper:

$$\min_{x} c_{G,1}^{T} x + x^{T}[c_{G,2}]x \tag{1}$$

subject to

$$F_{eq}x^{0} + f_{eq} = 0 \tag{2}$$

$$F_{neq}^{i}x^{i} + f_{neq}^{i} \leq 0 \tag{3}$$

for $i = 0 \dots N_{out}$, where $i = 0$ denotes the pre-contingency (base-case) and $i \neq 0$ denotes a post-contingency state. The equality constraints in (2) represent the power flow equations for the pre-contingency state. Dealing with linearized equations, we can express the deviation from the base case in the form of linear sensitivities. Hence, the pre-contingency and all post-contingency states are incorporated in (3), which ensures that line flow constraints, active power, and HVDC limits are satisfied. The decision vector x represents both the state variables, such as voltage angles, and the control variables, such as generators' active power, HVDC flows, etc. In the case of no corrective control actions, as in Sections III and VI, only the pre-contingency states are taken into account in (3), i.e. $x^{i} = x^{0}$. In Section IV, corrective control actions with HVDC lines are introduced, and, therefore, vector x^{i} includes decision variables for the different post-contingency states. The optimization minimizes the operating costs for the pre-contingency case, as shown in (1).

Different analysis objectives call for different implementations of this generic formulation. Thus, Section VI includes the voltage angles in the power flow equations, while Sections III and IV use a formulation which relates line flows to net power injections as described in [4], that is equivalent to a formulation based on Power Transfer Distribution Factor (PTDF) [5]. For the security constraints, Section VI uses the Line Outage Distribution Factors (LODF) [6] and the Generalized Generation Distribution Factors (GGDF) formulation [7], while the formulation of Section III is based on [4]. The different formulations are detailed in the respective sections.

III. SCOPF Formulations To Account For Forecast Uncertainty and Risk

III.A. Section Overview

In this section, we describe two improvements to the standard N-1 security assessment. First, we account for the forecast uncertainty from RES in-feed and loads in a comprehensive way, in order to avoid operating points that have either too low (dangerous) or too high (economically inefficient) security margins. Second, we propose a risk-based approach to the N-1 security assessment to account for both the probability and the severity of contingencies, in order to find a better compromise between operating cost and security.

Below, we present four different SCOPF formulations, summarized in Table I. The initial formulation is a standard DC SCOPF, including post-contingency constraints for single outages. We then extend the standard SCOPF formulation to a Probabilistic Security Constrained Optimal Power Flow

TABLE I
SCOPF NAMING CONVENTIONS USED IN THIS PAPER

		FORECAST UNCERTAINTY NO	FORECAST UNCERTAINTY YES
OUTAGE PROBABILITY	NO	standard SCOPF (Section III-B)	probabilistic SCOPF (Section III-C)
	YES	risk-based SCOPF (Section III-D)	risk-based probabilistic SCOPF (Section III-E)

(P-SCOPF), which guarantees with a chosen probability that the system will be N-1 secure despite deviations from the forecast. In the third part, the standard N-1 security constraints are replaced by risk-based constraints that utilize information about outage probabilities to set appropriate line limits, thus forming a risk-based SCOPF. The fourth formulation both accounts for forecast uncertainty and includes risk constraints, which gives us a risk-based P-SCOPF.

III.B. Standard SCOPF Formulation

The standard SCOPF formulation is based on [4]. We first focus on the power flow formulation, then describe how uncertainty is accounted for, and conclude with the resulting optimization problem.

a) Power flow formulation: We consider a power network comprising N_G conventional generating units, N_L loads, N_l AC lines, N_b buses, N_w wind power generators, and N_{DC} HVDC links. For the N-1 security analysis, we take into account any single outage involving the tripping of an AC line, load, conventional generator, HVDC line, or wind power generator. We denote the power outage index by $i = 0, 1, ..., N_{out}$, with '0' corresponding to the case of no outage and N_{out} denoting the total number of outages, i.e. $N_{out} = N_G + N_w + N_L + N_l + N_{DC}$. The power flows of the AC lines are given by $P_l = AP_{inj}$, where $P_{inj} \in \mathbb{R}^{N_b}$ is the net power injection at the buses. A is a constant matrix – equivalent to the PTDF matrix [5], [6] – that depends on the network topology. Following the notation in [4]

$$A = B_f \begin{bmatrix} (\widetilde{B}_{bus})^{-1} & \mathbf{0} \\ \mathbf{0} & 0 \end{bmatrix} \tag{4}$$

where B_f is the line susceptance matrix and $\widetilde{B}_{bus}$ the bus susceptance matrix without the last (arbitrarily chosen) column and row. Note that A changes following topology changes caused by line outages leading to an outage specific matrix A^i.

The equations for the HVDC links follow the formulations introduced in [8] and [9]. Each HVDC link is approximated by two virtual voltage sources located at the two nodes where the HVDC line is connected. For each HVDC link, we introduce one additional variable for the HVDC power flow. Let $P_{DC} \in \mathbb{R}^{N_{DC}}$ represent the vector of power flows on the HVDC lines. The balance between the active power injected into and withdrawn from the line is maintained by assuming that $P_{inj,m} = P_{DC,j}$ and $P_{inj,n} = -P_{DC,j}$ for an HVDC link j connected between nodes m and n.[1]

The wind power forecast error and certain component outages could lead to a generation-load mismatch in the system. Given this mismatch, the Automatic Generation Control (AGC) will drive the generation to a new operating point. Each generator adjusts its production compensating a percentage of the generation-load mismatch. In [4], the distribution vectors $d \in \mathbb{R}^{N_G}$ are introduced. Their elements denote the percentage with which each generating unit should change its production in response to the total mismatch. The post-disturbance generation operating point is given by $P_G - dP_m$, where $P_G \in \mathbb{R}^{\mathbb{N}}_{\mathbb{G}}$ denotes the power production of the generators and $P_m \in \mathbb{R}$ represents the generation-load mismatch.

b) Optimization problem: We aim to find a generation dispatch that minimizes generation costs while satisfying the network constraints for the base case and all post-contingency operating points. The generation cost vectors are denoted by $c_{G,1}, c_{G,2} \in \mathbb{R}^{N_G}$. $[c_{G,2}]$ is a matrix with vector $c_{G,2}$ on the diagonal. The resulting optimization is given by:

$$\min_{P_G} c_{G,1}^T P_G + P_G^T [c_{G,2}] P_G \tag{5}$$

subject to

$$\sum_{k=1}^{N_G} P_G^{(k)} + \sum_{k=1}^{N_w} P_w^{f,(k)} - \sum_{k=1}^{N_L} P_L^{f,(k)} = 0 \tag{6}$$

$$-\overline{P}_{DC} \leq P_{DC} \leq \overline{P}_{DC} \tag{7}$$

and for $i = 0, 1, ..., N_{out}$

$$-\overline{P}_l \leq P_l^i \leq \overline{P}_l \tag{8}$$

$$\underline{P}_G \leq P_G - d^i P_m^i \leq \overline{P}_G \tag{9}$$

where

$$P_l^i = A^i P_{inj}^i \tag{10}$$

$$P_{inj}^i = C_G^i (P_G - d^i P_m^i) + C_w^i P_w^f - C_L^i P_L^f + C_{DC}^i P_{DC} \tag{11}$$

$$P_m^i = -b_G^i P_G - b_w^i P_w^f + b_L^i P_L^f \tag{12}$$

Matrix C_G maps the vector of the generating units to the vector of the bus injections. Matrices C_w, C_L, C_{DC} are defined similarly. Constants b_G^i, b_L^i, b_w^i are binary row vectors whose elements are either '0' or '1'. A value of '1' corresponds to the tripped component for outage i. Note that the generation-load mismatch is equal to zero for the base case, $P_m^0 = 0$. For specific outages i it is non-zero and thus determined by the vectors b_G^i, b_L^i, b_w^i. Constraint (6) relates to the power balance equation for the deterministic case where the wind power infeed and the load consumption are equal to the forecasted values P_w^f, P_L^f.

[1] A formulation considering HVDC grids is presented in Section IV-C3.

III.C. Probabilistic SCOPF

The SC-OPF problem described in the previous section is deterministic in the sense that only the forecasted values of the loads and the wind power are taken into account. However, forecasts are typically error-prone, especially for wind power due to its fluctuating nature. Hence, it is meaningful to formulate stochastic variants of the SC-OPF problem as seen in [10], [11], [12], [13]. Most of these works model uncertain generation by means of scenarios without providing guarantees regarding the probability that the computed dispatch indeed satisfies the network constraints.

In [4], [14], an SC-OPF problem under uncertainty is formulated as a stochastic program with chance constraints enforcing line and generation capacity limits with a given probability. Such a formulation provides probabilistic guarantees of not violating line and generation limits. We refer to this setup as the probabilistic SC-OPF. A chance constraint (or probabilistic constraint) is typically given by:

$$\mathbb{P}\Big(h(x,\delta) \leq \overline{h}\Big) \geq 1-\varepsilon \tag{13}$$

where x denotes the decision variable, δ the uncertain variable and $\overline{h}$ a constant used as the upper bound of the constraint function $h(\cdot,\cdot)$. ε is a design parameter and denotes the probability with which the inequalities may be violated. Chance constrained problems are non-convex and in general difficult to solve with the exception of a few specific cases. When the forecast error is uniform or normally distributed, analytic approaches may be employed [15]. Such a setup has been developed for a probabilistic SC-OPF problems [14], [16]. It will be used in Section VI. However, in [4], the chance constrained problem is solved using a scenario approach [17], which does not require any assumption on the distribution of the forecast error. In this section, we follow the formulation of [4] and present a modification of the scenario approach based on [18] that has already been applied to probabilistic SC-OPF problems [19]–[21].

1. Optimization problem

We consider wind power generation and load uncertainty. The wind power forecast error is the difference between the actual wind power P_w and the forecast value P_w^f (i.e $\Delta P_w = P_w - P_w^f$). We assume that 90% of the load is constant and known, but that the remaining 10% is variable and uncertain, representing heating/cooling loads that consume power as a function of outdoor air temperature. Consequently, the total load is given by $P_L = P_{set} + P_T(T)$, with P_{set} denoting the constant part of the load and $P_T(T)$ the temperature dependent part. For the deterministic case we use $P_L^f = P_{set} + P_T(T^f)$. Hence, the load deviation from the forecast is defined by $\Delta P_L = P_T(T) - P_T(T^f)$. For simplicity, we assume only one temperature T for the overall system, though it would be straightforward to incorporate different temperatures for every load within the formulation.

We now formulate the probabilistic SCOPF problem, taking both the load and the wind power uncertainty into consideration. The initial problem is given by (5) - (9) with the following additional probabilistic constraint:

$$\begin{aligned}\mathbb{P}\Big(& -\overline{P}_l \leq P_l^i \leq \overline{P}_l \\ & \underline{P}_G \leq P_G - d^i P_m^i \leq \overline{P}_G \\ & \text{for all } i = 0, ..., N_{out} \Big) \geq 1-\varepsilon\end{aligned} \tag{14}$$

where

$$P_l^i = A^i P_{inj}^i \tag{15}$$

$$P_{inj}^i = C_G^i(P_G - d^i P_m^i) + C_w^i P_w - C_L^i P_L + C_{DC}^i P_{DC} \tag{16}$$

$$\begin{aligned}P_m^i = {} & k_w^i(P_w - P_w^f) - k_L^i(P_T(T) - P_T(T^f)) \\ & - b_G^i P_G - b_w^i P_w + b_L^i P_L\end{aligned} \tag{17}$$

Note, that the probability $\mathbb{P}$ in (14) is meant with respect the wind power $P_w \in \mathbb{R}^{N_w}$ and the temperature $T \in \mathbb{R}$. The inequalities in the chance constraint (14) are satisfied with a probability of at least $1-\varepsilon$. The inequalities inside the chance constraint correspond to Alternating Current (AC) line, generation and HVDC link limits, respectively. The elements of the row vectors k_w^i, k_L^i are either '0' or '1' with '1' corresponding to the components that are not tripped during outage i. Note that the power balance is trivially satisfied for all the uncertainty instances under the assumption that sufficient reserves are available to allow the generation-load mismatch to be compensated by the generator units according to the distribution vectors.

The aforementioned optimization problem can be written in a compact way in the form of (1)-(3) with the additional constraint

$$\mathbb{P}\Big(Fx + f + Hg(\delta) \leq 0\Big) \geq 1-\varepsilon \tag{18}$$

where x is a vector including the decision variables (here the generation dispatch P_G), and $\delta = [P_w \ T]^T \in \mathbb{R}^{N_w+1}$ is the vector of uncertain parameters, i.e. the realization of the power from every wind power generator and the realization of the temperature. Matrices F, H and vector f are of appropriate dimensions and are calculated based on (14)-(17). Note that (18) is in the form of (13).

2. Reformulation of the chance constraint

In this section, we describe how to solve the chance constraint problem without introducing assumptions on the probability distribution of the uncertainty and while providing guarantees regarding the probability of constraint satisfaction.

The discussion is motivated by [17] where the authors introduce a scenario approach to address chance constrained optimization problems. According to this approach, the chance constraint is substituted with a finite number of hard constraints corresponding to different scenarios of the uncertainty

vectors. Moreover, by using a sufficient number of scenarios it provides a-priori guarantees that the resulting solution satisfies the chance constraint with a certain confidence. In [22], it is shown that the number of scenarios that need to be generated is given by

$$N \geq \frac{1}{\varepsilon}\frac{e}{e-1}\Big(\ln\frac{1}{\beta}+N_x-1\Big) \tag{19}$$

where $\varepsilon \in (0,1)$ (see also (13)) is a violation parameter determining the desired probability level, $\beta \in (0,1)$ is a confidence level, e denotes the Euler number, and N_x denotes the number of decision variables. The solution of the optimization program involving only N scenarios is feasible for the chance constraint with a probability of at least $1-\beta$. Note that the number of the scenarios that need to be considered increases linearly with the number of the decision variables and hence the computational cost increases as well. This reformulation relies on the assumption that both the objective and the constraint functions are convex with respect to the decision variables, which is satisfied in our case.

An alternative scenario based methodology to deal with the chance constraint is proposed in [18]. This method includes two steps. In the first step, the scenario approach is used to determine, with a confidence of at least $1-\beta$, the minimum volume set that contains at least $1-\varepsilon$ probability mass of the uncertainty. Details on how to determine such a set can be found in [18], [19]. Here we denote this set by D. Its computation requires generating

$$N \geq \frac{1}{\varepsilon}\frac{e}{e-1}\Big(\ln\frac{1}{\beta}+2(N_w+1)-1\Big) \tag{20}$$

scenarios. Note that this bound does not depend on the number of decision variables as (19), but on the number of uncertainty variables which in our case is N_w+1.

In the second step, we use the probabilistically computed set D and formulate a robust problem where the uncertainty is confined in this set. The resulting optimizing problem is given by (1)-(3) and the chance constraint (18) is substituted by the following robust constraint

$$Fx+f+Hg(\delta)\leq 0, \text{ for all } \delta \in D \tag{21}$$

The interpretation of (21) is that the constraint should be satisfied for all values of $\delta \in D$. Following [18], any feasible solution of this robust problem is feasible for the chance constraint (18) with a probability of at least $1-\beta$. This guarantee arises from the fact that D is chosen in a probabilistic way. To solve the resulting robust program the reader is referred to [18], [23].

The constraints in the probabilistic SC-OPF formulation, as well as in most of the optimization problems presented in this paper, exhibit a specific structure that can be exploited to achieve a computationally simpler problem. Specifically, the uncertainty appears only in the terms $Hg(\delta)$ that are additive in the constraint functions and no bilinearities between the uncertainty elements and the decision variables exist. Therefore, it suffices to calculate off-line the maximum values of the elements of $Hg(\delta)$ as δ varies within D and replace with it the term $Hg(\delta)$ in the constraints. Specifically $Hg(\delta)$ is substituted with a vector whose elements are calculated as $\max_j H_k g(\delta^{(j)})$ with $j=1,\ldots,2^{N_w+1}$ denoting the indices of the vertices of the computed set D. Subscript k denotes the k-th row of matrix. The resulting problem is of the same size as each deterministic counterpart. This is also the case even if the standard scenario approach is employed. Since in both cases (scenario approach, two-step procedure) the complexity of the resulting problem is the same, in the probabilistic SC-OPF case study we use the two-step procedure becasuet it requires generating fewer scenarios. This follows from (19), (20) since in our case study $2(N_w+1)\leq N_x$.

III.D. Risk-based SC-OPF

In this section, we extend the standard SCOPF formulation to account for risk. The definition of risk incorporates not only the severity, but also the probability of an outage. Thus, a risk-based method addresses the second major driver of uncertainty in power systems operation, the probability of random failures. By utilizing this additional information, we can provide more detailed information on the security status of the system and find a better trade-off between security and cost. Risk-based OPF formulations have been proposed in the literature. [24] investigates different formulations with risk as part of the constraints and the objective. In [25], multi-objective optimization is proposed to optimize both system cost and risk. Furthermore, a measure for the risk related to cascading events is used to choose one of the pareto-optimal solutions. [26] proposes including additional constraints on the total system risk in an SCOPF with standard N-1 constraints.

The risk related to a given outage situation *i* and a given line *k* is

$$Risk_{i,k} = Pr_i \cdot Sev_{k|i} \tag{22}$$

where Pr_i is the probability of an outage i and $Sev_{k|i}$ is the severity of the situation at line k after the outage i has taken place. In order to evaluate the risk, the outage probabilities Pr_i must be estimated (e.g., based on historical data), and a suitable severity function $Sev_{k|i}$ needs to be defined. Depending on the choice of the severity function, different types of risk can be measured. Here, we focus on the risk related to transmission line overloading and use the severity function proposed in [26]. This function defines severity as a piecewise linear function of the line flow P_l

$$Sev(P_l) = \max\{-10P_l/\overline{P}_l - 9,\ 0,\ 10P_l/\overline{P}_l - 9\} \tag{23}$$

where $\overline{P}_l$ is the line limit. The severity is non-zero when the line flow is above 90% of the limit and increases linearly with the line flow. The severity function is depicted in Fig. 1.

In our view, there are three main risk limits that are of interest

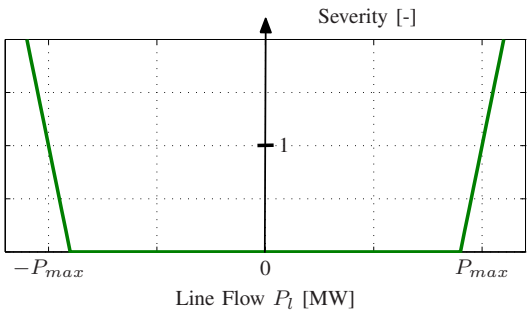

Fig. 1. Severity as a function of power flow on the line, based on [26].

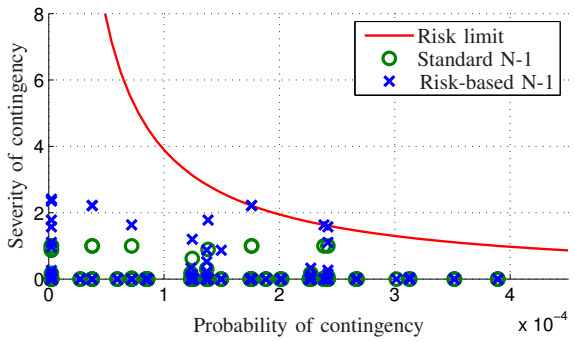

Fig. 2. Comparison between the severity of different contingencies for a standard and a risk-based N-1 dispatch.

in system operational planning

$$Risk_{i,k} = Pr_i \cdot Sev_{k|i}(P^i_{l,k}) \leq C_i \tag{24}$$

$$Risk_i = Pr_i \sum_k Sev_{k|i} \leq C_{cont} \tag{25}$$

$$Risk = \sum_i \sum_k Pr_i \cdot Sev_{k|i} \leq C_{tot} \tag{26}$$

where (24) constrains the risk for each component k in each post-contingency state i to stay below a constant limit C_i; (25) limits the risk of specific contingencies; and (26) limits the total risk in the system.

Here, we focus on the first type of constraints, which are component and contingency specific, similar to the standard N-1 constraints. Using (23) for the severity function $Sev_{i,k}$ and the notation introduced in Section III-B, we can reformulate (24) for the outage situations $i = 1, ..., N_{out}$

$$-\alpha \cdot \overline{P}_l \leq P^i_l \leq \alpha \cdot \overline{P}_l \tag{27}$$

where α represents a change in the line limits compared to the standard SCOPF, and depends on the contingency probability Pr_i and the risk limit C_i

$$\alpha = \left(0.1 \frac{C_i}{Pr_i} + 0.9\right) \tag{28}$$

To change the standard SCOPF formulation (5)-(9) into a risk-based formulation, we replace the standard N-1 constraints on the line limits (8) by their risk-based counterparts (27).

Constraint (27) is equivalent to the standard N-1 constraint if the constants C_i are chosen equal to the probability of the respective contingency, i.e. if $C_i = Pr_i$. However, choosing C_i differently for each contingency implies that we tolerate higher risk for some contingencies than for others. This highlights that the standard N-1 criterion results in inconsistent risk levels.

If the risk limit $C_i = C$ is the same for all contingencies, we get a tightening compared to the standard N-1 limits for the constraints where $C < Pr_i$, and a relaxation when $C > Pr_i$. For example, we can choose the limit $C = \max(Pr_i)$, since this is the maximum risk we allow for with the standard N-1 criterion. To illustrate the method, the severity of the post-contingency condition at different lines is plotted against the probability of the contingencies in Fig. 2. The outage probabilities and the severities were calculated based on a standard and a risk-based N-1 dispatch for the test system described in Section V-B, with C chosen equal to the highest line outage probability. The risk-based constraints allow the severity of the post-contingency line flows (blue crosses) to increase until the risk limit (red line) is reached. With standard N-1 constraints, the upper bound on the severity of the post-contingency line flows (green circles) is equal to 1, regardless of the probability of the contingency. This leads to lower risk, but increases cost.

III.E. Probabilistic Risk-based SCOPF

In the sections above, we presented two methods that improve two different aspects of the standard N-1 security assessment, a P-SCOPF formulation and a risk-based SCOPF. Here, we combine the two methods to form a risk-based P-SCOPF, accounting for both input uncertainties (as the P-SCOPF) and the probability of outages (as the risk-based SCOPF). A risk-based OPF formulation accounting for load uncertainty is also found in [24], although the formulation only considers the expected value of risk. We follow the approach in [27] and formulate the risk constraints as probabilistic constraints, in order to guarantee the enforcement of the risk limits with a chosen confidence level.

The optimization problem formulation is the same as for the P-SCOPF, but with the risk-based instead of the standard N-1 line limits inside the probabilistic constraint (14), resulting in

$$\begin{aligned} \mathbb{P}\Big(& -\alpha \cdot \overline{P}_l \leq P^i_l \leq \alpha \cdot \overline{P}_l \\ & \underline{P}_G \leq P_G - d^i P^i_m \leq \overline{P}_G \\ & \text{for } i = 1, ..., N_{out} \Big) \geq 1 - \varepsilon \end{aligned} \tag{29}$$

IV. SCOPF Formulations to Enhance Flexibility with Flexible Loads and HVDC Transmission Lines and Grids

IV.A. Section Overview

The four SCOPF formulations presented above incorporate uncertainty related to stochastic in-feed and random failures in operational planning. These methods rely on increased availability of information (about forecast errors and outage probabilities) and do not require any hardware changes. In contrast, we now discuss SCOPF formulations that increase system controllability via additional infrastructure, specifically flexible loads and HVDC links/grids. In doing so, we are able to quantify the effect of additional controllability on system security, operational costs, and maximum RES in-feed levels.

IV.B. Flexible Loads

1. Overview

Many types of electric loads have some degree of flexibility in terms of when they consume energy. Demand response programs harness this flexibility by providing incentives for loads to shift energy consumption in time. This sort of behavior can improve power market efficiency and power grid reliability. Here, we consider load scheduling in a day-ahead OPF. Load scheduling is different than generation scheduling because the exact amount of load flexibility may not be known in advance. Our contribution is to explicitly account for uncertainty in estimates of the flexibility of the controllable load and take that into account within a stochastic OPF framework.

2. Load modeling

We assume that loads can shift their consumption in time but that the total amount of energy delivered to the load over a period of time is fixed. Therefore, we model aggregations of loads as virtual storage units. Actions which decrease consumption relative to the baseline consumption (i.e. the consumption that would have occurred without scheduling) empty the unit and actions with increase consumption relative to the baseline consumption charge the unit. Therefore, the energy state S of the aggregation evolves as

$$S_{t+1} = S_t + (P_{C,t} - P_T(T_t))\Delta\tau, \tag{30}$$

where $P_{C,t}$ is the mean power consumption of the controllable portion of the load at time step t and also the optimization variable, $P_T(T_t)$ is the baseline consumption, and $\Delta\tau$ is the length of the time step.

Because the amount of controllable load within the system varies as a function of time, the size of the virtual storage unit is time-varying. Specifically, a virtual storage unit's power and energy capacity are a function of a variety of time-dependent quantities such as ambient conditions and human behavior. Therefore, both P and S are constrained by time varying quantities:

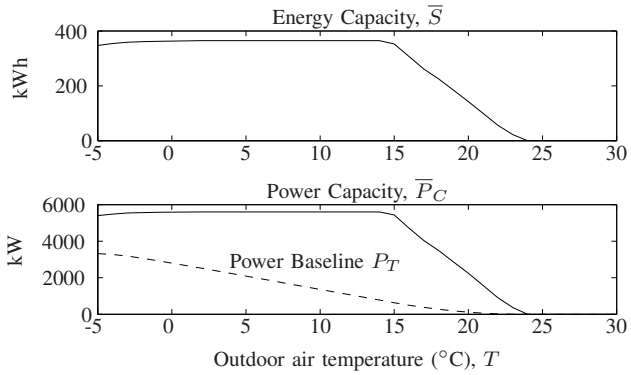

Fig. 3. The power and energy capacity of an aggregation of electric heaters modeled as a virtual storage unit.

$$\underline{P}_C(T_t) \leq P_{C,t} \leq \overline{P}_C(T_t) \tag{31}$$

$$0 \leq S_t \leq \overline{S}(T_t) \tag{32}$$

where $\underline{P}_C(T) + \overline{P}_C(T)$ is the aggregate power capacity and $\overline{S}(T)$ is the aggregate energy capacity. Ref. [28] describes a method of computing $\underline{P}_C(T)$, $\overline{P}_C(T)$, and $\overline{S}(T)$ for an aggregation of residential electric heaters or air conditioners as a function of outdoor air temperature T. We use this method here to compute values for an aggregation of 1,000 electric heaters as shown in Fig. 3. Here we assume $\underline{P}_C(T) = 0$ for all outdoor air temperatures.

There are many reasons why P_T, $\underline{P}_C$, $\overline{P}_C$, and $\overline{S}$ may be uncertain including model error and forecasting error [29]. Here, we do not consider all sources of uncertainty but instead focus on just one cause: temperature forecasting error. Specifically, we assume that the values in Fig. 3 are accurate for a given outdoor air temperature but that our forecasts of outdoor air temperature are uncertain. Given a specific forecast of outdoor air temperature, we can use Fig. 3 as a look-up table to determine the expected power and energy capacity of a virtual storage unit for planning; however, the actual outdoor air temperature will dictate the actual capacities available in real-time.

3. Optimization problem

Since loads have inter temporal constraints, we formulate the full multi-period problem, though in the case study we only solve for one period so that our results are comparable to those generated with the other formulations. We pose the following optimization problem in which we augment the probabilistic SC-OPF problem of Section III-C to include hourly steps (denoted by t) and assume preventive control actions are

possible with controllable loads:

$$\min_{\{P_{G,t},P_{C,t}\}_{t=1,..,N_t}} \sum_{t=1}^{N_t} \left(c_{G,1}^T P_{G,t} + P_{G,t}^T [c_{G,2}] P_{G,t} \right) \quad (33)$$

subject to

$$\sum_{k=1}^{N_G} P_{G,t}^{(k)} + \sum_{k=1}^{N_w} P_{w,t}^{f,(k)} - C_L^0 (P_{L,t}^{set,(k)} + P_{C,t}^{(k)})) = 0 \quad (34)$$

$$-\overline{P}_{DC} \leq P_{DC,t} \leq \overline{P}_{DC} \quad (35)$$

$$\begin{aligned} \mathbb{P} \Big(& -\overline{P}_l \leq P_{l,t}^i \leq \overline{P}_l \\ & \underline{P}_G \leq P_{G,t} - d_t^i P_{m,t}^i \leq \overline{P}_G \\ & \underline{P}_C(T_t) \leq P_{C,t} \leq \overline{P}_C(T_t) \\ & 0 \leq S_t \leq \overline{S}(T_t) \\ & 0 \leq S_{\tau+1} \leq \overline{S}(T_\tau) \\ & \text{for } i = 0, ..., N_{out}, \quad t = 2, \ldots, N_t \\ & \text{and } \quad \tau = 1, \ldots, N_t - 1 \Big) \geq 1 - \varepsilon \end{aligned} \quad (36)$$

where

$$\begin{aligned} S_{t+1} &= S_t + (P_{C,t} - P_T(T_t))\Delta\tau \\ P_{l,t}^i &= A^i P_{inj,t}^i \\ P_{inj,t}^i &= C_G^i (P_{G,t} - d_t^i P_{m,t}^i) + C_w^i P_{w,t} \\ &\quad - C_L^i (P_{L,t}^{set} + P_{C,t}) + C_{DC}^i P_{DC,t}, \\ P_{m,t}^i &= k_w^i (P_{w,t} - P_{w,t}^f) - b_G^i P_{G,t} - b_w^i P_{w,t} \\ &\quad + b_L^i (P_{L,t}^{set} + P_{C,t}) \end{aligned} \quad (37)$$

We also impose a set of deterministic constraints that represent a deterministic variant of (36) corresponding to the case where $P_{w,t} = P_{w,t}^f$ and $T_t = T_t^f$. These constraints are not repeated here for the ease of notation. The first two constraints inside the probabilistic constraint correspond to the line and generation limits as defined in Section III-C. The rest of the constraints inside the probabilistic constraint correspond to the aggregated power and energy capacity limits as described in (31), (32). The aforementioned problem remains in the form of (1)-(3), (18), and we solve it using the two-step scenario based methodology as described in Section III-C2.

Note that when we solve only a single period optimization with this formulation, the optimizer attempts to minimize the load as much as possible given constraints (31), (32). This means that only the uncertainty in P_T and $\underline{P}_C$ is important for this problem. In the multi-period case, the uncertainty in $\overline{P}_C$ and $\overline{S}$ would also be important.

IV.C. VSC-HVDC Technology

1. Overview

Increased integration of RES in remote areas requires the building of new transmission lines to transfer renewable power to load centers. HVDC lines are attractive options as they incur less losses over long distances, while enhancing the controllability of the power grid. The focus in this section is on HVDC lines based on Voltage Source Converter technology (VSC-HVDC), which allow independent control of active and reactive power flow. If appropriately controlled, VSC-HVDC can enhance power system security in a variety of ways, for example, by providing voltage support during steady-state operation [30].

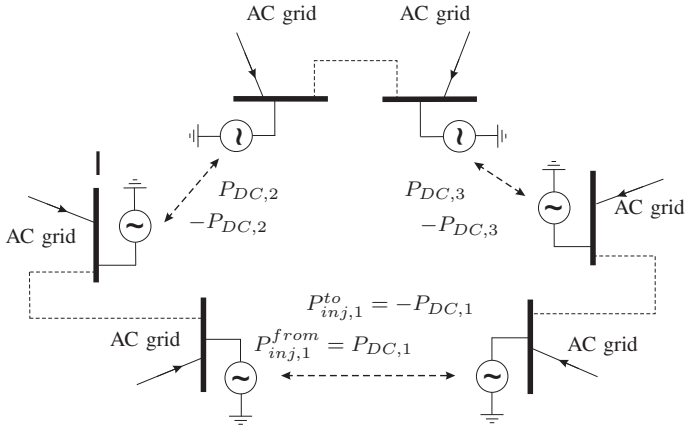

Fig. 4. Equivalent circuit for three PTP VSC-HVDC lines in a DC-OPF context. One decision variable $P_{DC,i}$ is used for each PTP HVDC link. This topology allows for a higher degree of power flow controllability, but it also results in higher investment costs (more converter stations compared with the HVDC grid).

By actively changing their power flow, HVDC lines are able to undertake both preventive and corrective control actions. Thus, we can formulate an SCOPF to not only determine their operating point for the base case (see (7), (11)), but also determine the change in HVDC power flow needed after a contingency occurs to maintain system security. In [31], such a security-constrained OPF is proposed, based on an AC-OPF formulation. It includes the post-contingency control of VSC-HVDC lines and demonstrates the benefits in terms of cost savings resulting from the ability of HVDC lines to act correctively.

In addition to Point-to-Point (PTP) solutions, where the ends of each HVDC line are connected to AC nodes, the VSC-HVDC technology enables the formation of an HVDC grid. This paper includes both topologies in the SCOPF formulation and compares their performance in the case study presented in Section V. Figures 4 and 5 present the modeling approach for the two topologies.

In this paper, the capability of corrective control actions has been incorporated only in the case of PTP HVDC links. Future work will include corrective control actions for the case of HVDC grids. In Section IV-C2, the formulation for PTP HVDC lines is described, while Section IV-C3 focuses on multi-terminal HVDC grids.

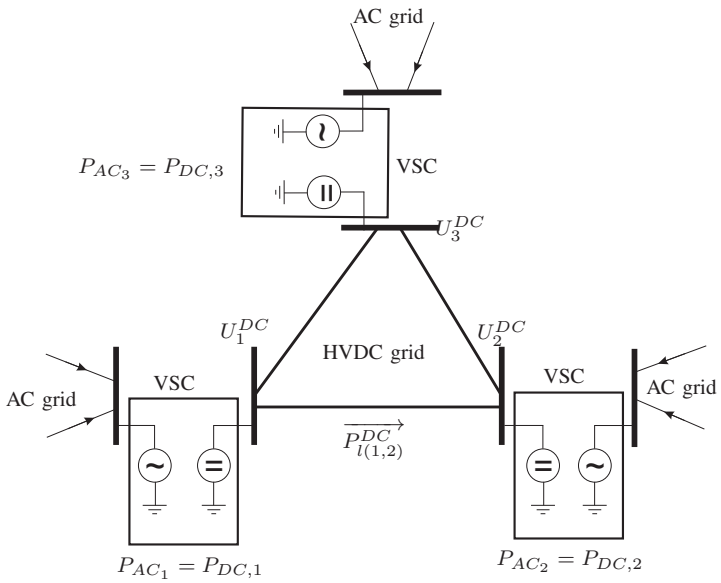

Fig. 5. Equivalent circuit for Multi-Terminal HVDC grids in a DC-OPF context.

2. VSC-HVDC Point-to-Point Links

We described our method for including PTP HVDC links in Section III-B. Here, we augment the probabilistic SCOPF to include HVDC corrective control actions. We assume that for any outage the HVDC power flow setpoint can be adjusted accordingly. This adjustment is represented by a set of variables $K^i \in \mathbb{R}^{N_{DC}}$ for all $i = 1, ..., N_{out}$. Specifically, the post-contingency setpoint is given by $P_{DC} + K^i$.

The probabilistic SCOPF including the corrective control action of the HVDC links is given by (5), (6), (8), (9), (14) with the additional constraint:

$$-\overline{P}_{DC} \leq P_{DC} + K^i \leq \overline{P}_{DC}, \quad i = 1, ..., N_{out} \tag{38}$$

In the case study presented in Section V we show that HVDC corrective control actions decrease the operational costs and can defer investments in additional AC lines when higher shares of wind power need to be integrated.

3. Multi-terminal HVDC grids

Multi-Terminal DC Grid (MTDC) grids have two major benefits over PTP links. First, each end of a PTP HVDC link needs a VSC station whereas MTDC grids needs only one VSC at each HVDC bus. Even if the capacity of the VSC stations in an MTDC grid are higher than in a system with PTP links, the investment cost could be significantly lower as less installations are needed. Second, the operation of MTDC grids can be decoupled from that of the AC grid when there are line outages. Therefore, the effects of an HVDC line breakdown will not disturb the AC grid and vice versa. However, one disadvantage of MTDC grids is that, with fewer VSCs, the system is less controllable than systems with PTP links.

The SCOPF formulation described in Section III-B was extended to incorporate MTDC grids. To maintain power balance, we set the power flow through the converters $P_{DC,c}$ to be equal on the AC side and HVDC side. Since we can control the flow through the terminals, the flows are added to the decision vector x. The voltages in the MTDC grid are defined in relative values to a reference voltage, similar as it is done for the angles in the AC grid in the standard DC-OPF formulated in [32]. Therefore, the flow equation

$$P_{l(m,n)}^{DC} = \frac{U_m^{DC}(U_m^{DC} - U_n^{DC})}{R_{m,n}} \tag{39}$$

can be linearized to

$$P_{l(m,n)}^{DC} = \frac{U_m^{DC'} - U_n^{DC'}}{R_{m,n}} \tag{40}$$

This simplification results in a lose of accuracy, but also results in significant gains regarding the calculation speed. Losses in the MTDC grid are not explicitly considered (consistent with the SCOPF formulation described Section III-B). To implement the method, the formulation in (5)-(10) is extended by adding power balance equations for each HVDC bus. The maximum power flows through the VSC stations are represented with additional inequalities. The limits for HVDC lines are added as security constraints to compensate for line outages inside the MTDC grid. A detailed description of the used calculation method is described in [33].

V. Case Study - Single Area System

V.A. Section Overview

In the following case studies, the applicability of the previously developed formulations is demonstrated on the three-area RTS-96 system. First, we quantify how N-1 security as well as uncertainty increase operational costs. Next, we demonstrate how this cost rise can be countered by risk-based security concepts in conjunction with control schemes taking advantage of the controllability of generators, loads, and HVDC technology. We also show how the controllability of these elements could maximize the RES in-feed and defer investments in new transmission lines.

V.B. Test System

The different SCOPF formulations are demonstrated on the IEEE Three Area RTS-96 system, as described in [34], with some modifications. We added aggregations of wind power in-feed to three different buses, listed in Table II. We also made two modifications to the topology. For the case study in Section V-C, the HVDC link of the original system was

TABLE II
WIND GENERATION

Bus #	108	115	213
Forecasted Wind Power [MW]	425	1270	700

TABLE III
POSITIONS OF GRID REINFORCEMENTS, EACH WITH 300 MW CAPACITY

Line #	1	2	3	4	5	6	7	8
From	109	109	115	115	210	210	216	309
To	115	210	216	316	216	309	316	316

replaced by two HVDC links between buses 109-115 and 216-316, each with a capacity of 300 MW. For the case study in Section V-D, we use a number of additional reinforcements, detailed in Table III. Both system configurations are shown in Fig. 6. We consider a peak load situation, where the total system load equals 8550 MW and the total dispatchable generation capacity (not including wind energy) is 10215 MW.

The probabilistic formulations are solved using the two-step scenario-based methodology presented in Section III-C2. There are $N_w + 1$ uncertain variables, corresponding to the number of wind power in-feeds and the temperature. To ensure a violation probability of maximum $\varepsilon = 0.1$ with a confidence level $\beta = 10^{-4}$, we need to consider 257 scenarios, as given by (20). The scenarios are generated under the assumption that the wind power in-feed and the temperature are independent, which allows us to use different models for each. For the wind power scenarios, we use the Markov chain mechanism described in [35]. We use normalized forecasted and actual hourly wind power data for Germany over the period 2006-2011. Following [35], we discretize the error between the forecast and the actual data to "train" the transition probability matrix, enabling us to generate various wind power scenarios. For the temperature scenarios, we use 1 year of hourly forecast and actual values from data of 11 sites in Switzerland to represent possible temperature forecast errors. In our single period SCOPF, we assume the temperature is 13°C and then add the vector of forecast error to represent the temperature scenarios.

For the risk-based methods, we select the risk limit equal to the highest line outage probability. The outage probabilities are calculated based on the reliability information in IEEE RTS96. To compute the numerical solutions to the problems, we use the solver CPLEX via the MATLAB interface TOMLAB.

V.C. Operation Schemes

1. Operating Costs

In this case study, we investigate the cost of generation dispatch for different SCOPF formulations incorporating different levels of forecast uncertainty and controllability. We also compare standard N-1 security to risk-based security criteria. We consider the IEEE RTS96 system with two HVDC links and a situation with 80% of the wind in-feed listed in Table II.

Figure 7 shows the cost of generation dispatch for the different SCOPF formulations presented in the previous sections. We compare each cost to that resulting from a normal OPF, where no contingency-related constraints are included. The two lines denote the standard N-1 formulation and the risk-based N-1 formulation. As we move towards the right, every point represents a further extension of the algorithm. Beside the standard OPF and SCOPF formulations, we include two levels of uncertainty (leading to increasing costs) and two levels of controllability (leading to decreasing cost).

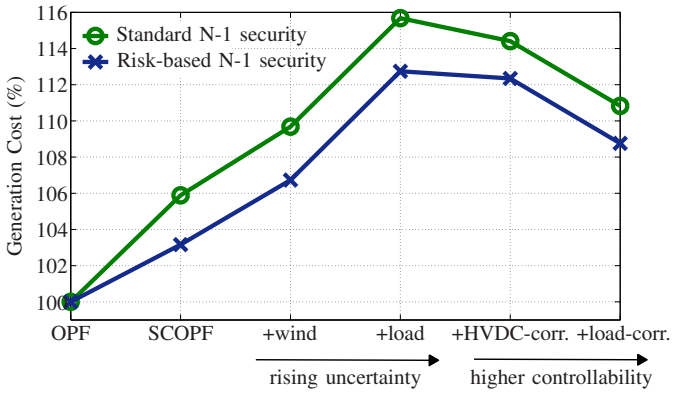

Fig. 7. Dispatch cost with different SCOPF formulations, as a percentage of cost associated with an OPF. SCOPF: standard SCOPF; +wind: P-SCOPF with wind uncertainty; +load: P-SCOPF with both wind and load uncertainty; +HVDC-corr.: P-SCOPF with wind and load uncertainty, and corrective control actions with HVDC links; +load-corr.: P-SCOPF with wind and load uncertainty, and corrective control actions with HVDC links and controllable loads.

First, we will discuss the results obtained assuming the standard N-1 criterion (green curve), and afterwards move on to the risk-based formulation (blue curve). The standard SCOPF, which includes N-1 constraints, increases cost by 6% compared to the benchmark OPF solution. Extending the formulation to a probabilistic SCOPF including wind uncertainty (denoted "+wind"), the cost increases by another 4%. Including load demand uncertainty due to temperature forecast errors (denoted "+load"), increases operating costs by another 6%. The cost increase arises from the tightening of the constraints which is necessary to secure the system against the uncertainty associated with wind power in-feed deviations.

On the other hand, controllable line flows and flexible demand help counteract this increase in the operating costs. As shown in Fig. 7, the corrective control capabilities of the HVDC lines can decrease operating costs by about 1.5% (denoted "+HVDC-corr."), while flexible demand response can reduce operating costs by a further 4% (denoted "+load-corr.").

Considering now the risk-based formulation (blue curve in Fig. 7), we observe that the operating costs follow a trend similar to the standard N-1 criterion as more degrees of uncertainty and controllability are taken into account. However,

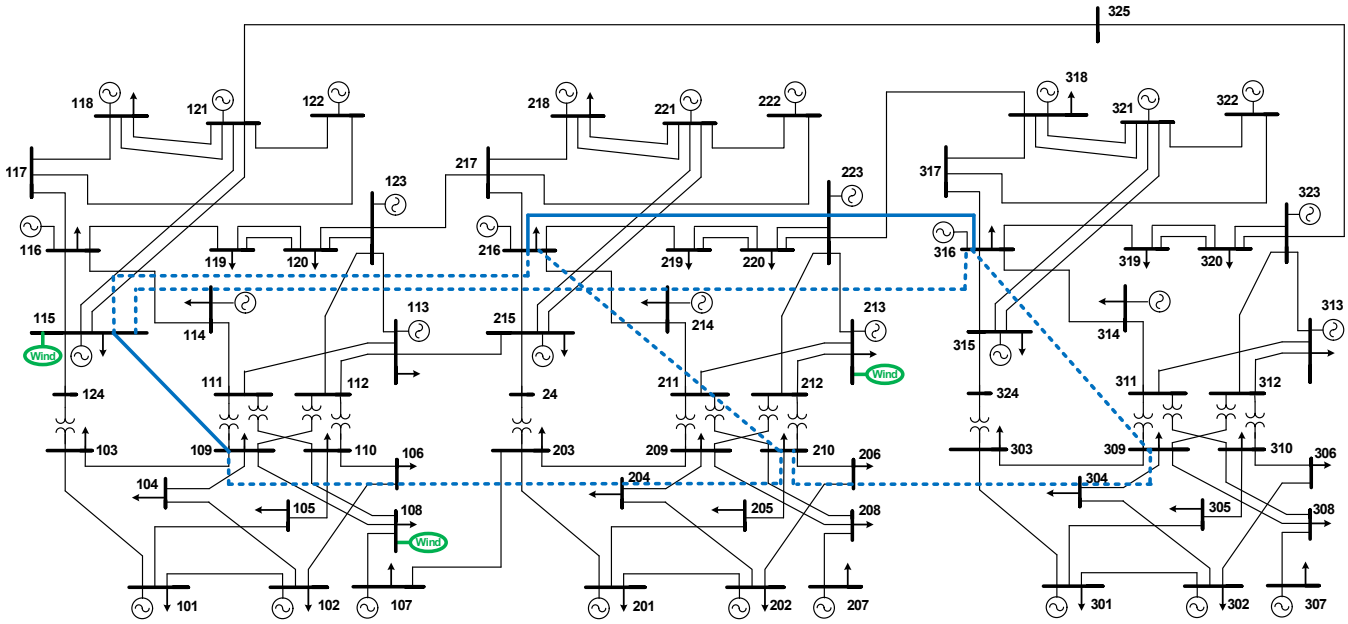

Fig. 6. IEEE RTS96 Test system with three areas. The grid reinforcements that are part of all case studies are marked with blue lines, while the grid reinforcements only part of the case study in Section V-D are marked with blue dashed lines.

we find that replacing the standard line limits by the risk-based line limits in (27) leads to a cost decrease on the order of 2%-3% for all SCOPF formulations. This is not surprising when we consider that all but one line limit is relaxed when we select the maximum risk allowed in the deterministic N-1 case as the overall risk level.

The cost increase induced by the probabilistic constraints is the price we pay for higher security. We check 10,000 different scenarios for the wind energy in-feed to determine if there are any constraint violations. Without considering uncertainty in the SCOPF formulation, the pre-contingency dispatch results in violations in 100% of the different wind in-feed scenarios. With a probabilistic SCOPF formulation, whether it is based on the standard or the risk-based N-1 criterion, the pre-contingency dispatch results in violations in less than 0.2% of the scenarios. Considering that the chosen confidence level is 10%, the scenario approach is relatively conservative. However, this is in line with results presented for similar approaches [4].

Concluding this case study, we observe that ensuring the security of the system under uncertainty in generation and/or demand results in up to 10% higher operating costs – independent of the applied security criterion, i.e. deterministic vs. risk-based N-1. At the same time, corrective control capabilities offered through HVDC lines or flexible demand, have the potential to manage the forecast error uncertainty in RES in-feed and demand. We find that they can limit the increase in operating costs to about 50% of the original value. It should also be noted that risk-based security criterion can not only provide a better metric for the severity of each contingency, but it can also result in lower costs by applying the same level of risk to all contingencies.

2. *Wind Power Penetration*

In this case study, we compute the maximum wind in-feed that can be integrated into the system, without violating any security constraints. Our goal is to investigate to what extent the corrective control capabilities of the HVDC lines can defer investments in new AC lines.

To calculate the maximum wind penetration in the system, we developed a variant of the probabilistic SCOPF problem presented in Section III-C. Specifically, we augment the decision variables to include both the generation and the wind power forecast. In this problem, we no longer minimize the generation costs but, instead, we maximize the sum of the wind power forecasts. In this case, the constraint functions include products of the decision variables and the uncertainty. Therefore, we can no longer use one vector to replace $Hg(\delta)$ since the uncertainty is not additive. This problem is computationally more complex since we need to add constraints for each scenario. To solve the problem, we use again the two-step scenario-based methodology, described in Section III-C2, which requires us to take into account considerably less scenarios than the standard scenario approach.

Here, we compare HVDC controllability against new AC line reinforcements. The placement of the additional AC lines was based on a heuristic approach. Starting from the base case, i.e. P-SCOPF with wind uncertainty, and assuming the maximum wind in-feed, we calculate the Lagrangian Multiplier (LM) of the line flow constraints. The LMs are sensitivities representing the marginal decrease in operating costs if one additional MW were allowed to flow through the line. High line LMs mean that reinforcing these lines will result – marginally – in high cost savings. Along the line with the highest LM, we

place a parallel AC line with the same characteristics, in the form of a line reinforcement. We increase the maximum wind in-feed step-wise until the problem becomes infeasible. At the last feasible step, we calculate again the values of the line LMs and we place a parallel line along the path with the highest LM.

Figure 8 shows results that are based on the RTS96 system with two HVDC links. For the AC reinforcements, the first additional AC line is line 107-108, while the second line connects nodes 211-213. As seen, the probabilistic SCOPF

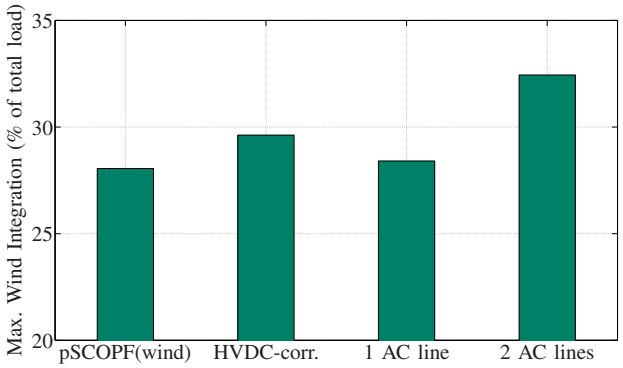

Fig. 8. Maximum wind integration: comparison between HVDC controllability and the installation of new AC lines. pSCOPF(wind): probabilistic SCOPF with wind uncertainty; HVDC-corr: pSCOPF(wind) including corrective control actions of HVDC lines; 1 AC line: pSCOPF(wind) with one additional AC line (between nodes 107-108); 2 AC lines: pSCOPF(wind) with two additional AC lines (between nodes 107-108, 211-213).

with wind uncertainty results in a maximum wind share of 28%. By allowing the existing HVDC lines to offer corrective control actions, the maximum wind in-feed rises to a share of about 30%. In the absence of HVDC corrective control, at least two additional AC lines would be necessary in order to achieve an equal or higher share of wind integration. This case study highlights that taking advantage of the controllability offered by existing infrastructure can have an effect equivalent to transmission expansion measures. Advantages here are that no additional investment costs would be incurred and the long licensing procedures for the building of new lines would be avoided.

V.D. Expansion Options

1. Operating Costs

In this case study, we compare the operation costs of different network reinforcement scenarios. Specifically, we use the P-SCOPF formulation with uncertain wind in-feed to evaluate the costs associated with adding new lines (Table III and Fig. 6), each with a transfer capacity of 300 MW. We first assume all new lines plus all existing HVDC links are AC lines. This increases transfer capacity, but has no influence on controllability. Second, we assume all new lines are PTP

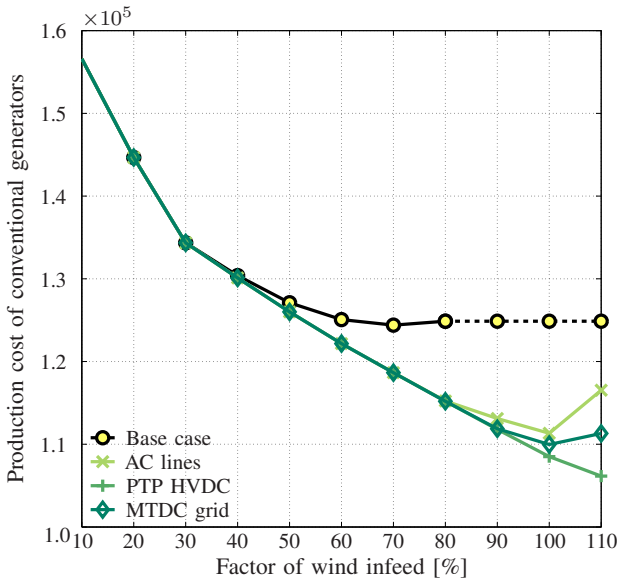

Fig. 9. Comparison of operation costs for grid reinforcements with AC lines, PTP HVDC lines, and MTDC grids. The base case without any HVDC links is infeasible for more than 80% wind in-feed.

HVDC links, with VSCs at the end of each link. Finally, we assume the new lines are part of an MTDC grid, where each DC bus within the grid has one VSC station. We compare each of these cases to a base case, which does not include any additional lines and removes the existing HVDC links. The operation cost are calculated for different scenarios of wind in-feed. Specifically, we assume the in-feeds to be 10% to 110% of the values in Table II, and we scale each wind farm by the same factor.

Results are shown in Fig. 9. The base case and all reinforcement measures achieve the same results up to 30% wind power in-feed. Since wind power in-feed has zero marginal cost, generation costs decrease with increasing wind in-feed. Beyond 40% wind in-feed, the reinforcement measures achieve lower operating costs than the base case. The base case reaches its minimum operation cost at 70% wind in-feed and can not accommodate more than 80% wind in-feed. When the in-feed is greater than 80% it must be curtailed to ensure secure operation. In contrast, the reinforced grid can be securely operated up to wind in-feed levels of 110% regardless of the reinforcement technology. The operation costs associated with the different technologies start to diverge at 90% wind in-feed. For additional AC lines and the MTDC grid, we see an increase of cost at 110% in-feed because the security costs are higher than the savings realised by the additional wind generation. The PTP HVDC system gives the most promising results for this case study, with the lowest cost at high levels of wind in-feed. However, we should keep in mind that this is the most expensive solution to construct. For the PTP link reinforcement scenario, 16 VSCs are needed, compared with only 6 in the MTDC grid case. Additionally, the PTP HVDC links negatively influence the existing AC grid during outages, which is not (necessarily) the case with an MTDC grid failure.

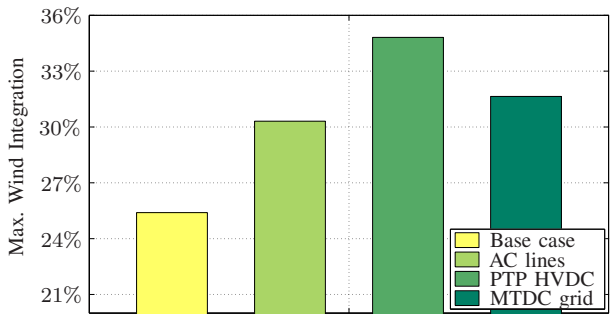

Fig. 10. Comparison of maximum wind in-feed for grid reinforcements with AC lines, PTP HVDC lines, and MTDC grids.

2. Wind Power Penetration

This case study investigates the maximum achievable level of wind in-feed for each of the reinforced grid scenarios described in the previous subsection. In this case, we increase the production capacities of the three wind farms until the problem becomes infeasible. Figure 10 shows that the base case results in the least potential to connect wind generation, followed by the scenario with additional AC lines. We find that with PTP links the grid can take more wind in-feed than with a MTDC grid.

VI. Operation of Multi-Area Systems

VI.A. Section Overview

Until now we have focused on systems which are operated by a single TSO. However, in reality, this is the case for few systems. The focus of this section is on the operation of interconnected Multi-Area System (MAS), which are systems which are tightly connected but operated by separate entities. This differentiates them from single area systems which are physically and operationally independent of other systems. In Europe, the growth of MAS was driven by the interconnection of the national power grids. This increased security and availability of the system by allowing cooperation between grid participants. The interconnection of the areas leads to lower costs for generation as capacity can be allocated across borders, and thus shared more efficiently.

Since in MAS multiple TSOs operate the grid, a number of issues may arise. The operation of the areas is separated along the borders of each area, and so operators may not be able to fully monitor and manage power flow across borders. Additionally, an operator of one area may have incomplete information about the other areas, i.e. to him the system is partially observable. For example, he may not know the full grid topology or he may not know the RES in-feed forecast errors because he does not know the actual wind power production in the other areas.

TABLE IV
NAMING CONVENTIONS FOR FULLY AND PARTIALLY OBSERVABLE MAS

Observability of		**RES FORECAST ERROR** FULL	PARTIAL
TOPOLOGY	FULL	fully observ.	partial-error
	PARTIAL	partial-topology	partially observ.

The OPF and SCOPF formulations for MAS are similar to the formulations used for single-area systems. In the OPF formulation, the operation costs are minimized subject to the power balance, generator limits, and power flow constraints. In the SCOPF formulation, the N-1 criterion is added to the optimization problem. In MAS, tie-line faults are not included in the list of credible contingencies. In this section, we consider cases of high RES in-feeds and so we formulate P-SCOPFs for fully and partially observable MAS. We consider observability of both topology and RES in-feed forecast error; our naming conventions for the various scenarios are shown in Table IV. We describe how to account for partial system knowledge, and how this affects the solutions.

VI.B. Reformulating the P-SCOPF chance constraints assuming normally-distributed RES in-feed errors

In P-SCOPF formulations for MAS, the uncertainty of power flows is handled by increasing the security margin of the lines. In this section, we describe how to calculate these margins assuming normally-distributed RES in-feed forecast errors. This allows us to use an analytic reformulation of the probabilistic constraints (13). In the case study, we use this approach to analyze MAS in which RES in-feed forecast error is fully and partially observable.

In this section, we formulate separate probabilistic constraints for every single line. This is in contrast to the previous formulation that included joint constraints (18). A drawback to this method is that the quality of the results is a function of the accuracy of our error distribution assumptions and how we can approximate the variance.

We use the DC power flow approximation and PTDFs [36] to model the distributed slack bus. We assume that the forecast is unbiased so that the mean value of the forecast error is zero, and we estimate the variances from historical data. For linear models, where the input quantities are normally distributed, the variance of output quantities may be calculated based on input variances [37]. Thus, the variances of power flow distributions of lines may be computed from the variances of the wind forecast errors. Importantly, the variances depend on the system topology and so they must be recomputed for each contingency case.

The power flow distribution of line k after contingency i is given by the normal distribution $h_{ik}(x)$, with a mean

calculated based on the forecasted values and the variance computed as explained above. We now formulate separate probabilistic constraints for the line flows, where each line limit is enforced with a given probability. With the assumption of a normal distribution and separate probabilistic constraints, we can express the effect of the uncertainty as a tightening of the capacity limit of the lines [14], [16]. This leads to the following new capacity limit for line k after a contingency i

$$\overline{\tilde{P_l^i(k)}} = \overline{P_l(k)} - \Delta P_l^i(k) \tag{41}$$

The decrease of the power flow limit $\Delta P_l^i(k)$ depends on the normal distribution h_{ik} and is

$$\int_{-\infty}^{\Delta P_l^i(k)} h_{ik}(x)dx = 1 - \varepsilon \tag{42}$$

This decrease in the power flow limit is exactly the decrease which is needed to make sure that the line constraint is enforced with a probability of $1 - \varepsilon$, as illustrated in Fig. 11.

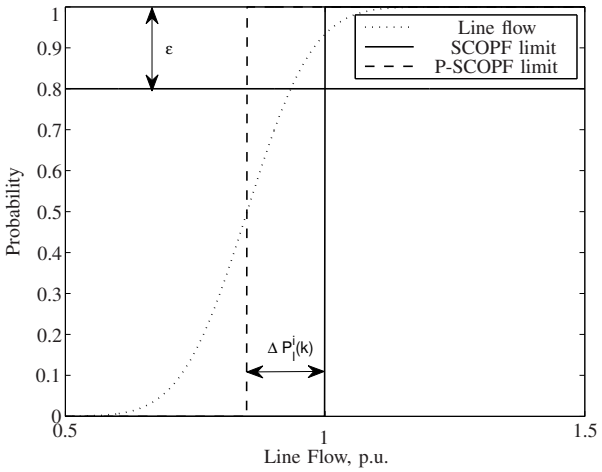

Fig. 11. Adjustment of line limits in order to consider the forecast errors of wind in-feed in operational planning. The physical line limit (1 p.u.) used in the SCOPF is decreased for the probabilistic SCOPF in order to fulfill the given probability that the power flow of the line does not exceed the physical line limit at the moment of supply.

VI.C. Distributed OPF Calculation in MAS

1. Motivation

The motivation for not sharing full information between grid operators is primarily a regulatory and confidentiality one. A solution which is determined by a single entity, having full knowledge of the system, is the optimum solution - there is no mathematical benefit to splitting the problem. For example, the line flows calculated within an area without considering the external grid are higher than the actual flows, reducing the ability of the system to accommodate post-contingency flows.

In this section, we consider how the various SCOPF-formulations can be separated so that different TSOs can solve different parts of the problem based upon knowledge of only the system topology within their area. Compared to [38], this paper presents a decentralized formulation with a weaker area coupling. Specifically, the formulation considers only the import, or export, of energy taking place at the border nodes at a price communicated by the neighboring area. It does not take into account the angles on the border nodes. This weaker coupling enables interconnections using different technologies, such as HVDC and AC lines, or even an MTDC grid.

2. Formulation

The formulation used in this section is different from the formulations in other parts of the paper. Instead, we base our decentralized calculation on a standard OPF problem, as defined in [32]. The decentralized solution of the problem is performed by an iterative search for an agreement on the cross-border power flow and the price for these flows. In previous formulations [39]–[41], the nodal angles were also in agreement; however, this state is not considered here. The general solution of the iterative procedure is:

while *true* **do**
  Calculate optimal generation dispatch
  Calculate LM for border nodes
  Exchange data with neighboring systems
  if *Termination criteria reached* **then**
    end;
  end
end

The cost-function of the decentralized formulation is a Quadratic Programming (QP)-OPF problem with auxiliary variables for the imported power

$$\min_{[P_G,P_I,\theta,P_N]} c_1(P_G) + c_2(P_I) + c_3(\theta) + c_4(\Delta) \tag{43}$$
$$c_1(P_G) = P_G^T[c_{G,2}]P_G + c_{G,1}P_G$$
$$c_2(\theta) = \theta^T W_{rr}\theta$$
$$c_3(P_I) = \kappa P_I$$
$$c_4(\Delta) = \begin{bmatrix} P_I & P_N \end{bmatrix} \begin{bmatrix} 1 & -1 \\ -1 & 1 \end{bmatrix} \begin{bmatrix} P_I \\ P_N \end{bmatrix}$$

The internal states are the power generation P_G at each node and the voltage angle θ relative to a reference node in each area. Further, the states of the border nodes are given by the power exchange P_I desired by the area, and the power exchange desired by the external area P_N. The decision vector for the decentralized problem is thus $x = [P_G, P_I, \theta, P_N]$. The additional cost $c_1(P_I)$ is the cost for import, or profit from export, and $c_4(\Delta)$ is a penalization term for the difference between the internal state and the state sent by the external area. This drives the values of the border nodes toward each other. The term $c_2(\theta)$ acts as a proxy for the power flow losses.

The value κ, the price for imports, is given by the LMs of the power equality constraint on the border nodes. The cost of imports is the cost of exports from the neighboring system; as such κ is an input from the neighboring system.

The power flow equations are solved based on the nodal angle difference, given as $P_l = B_f\theta$, where B_f is the susceptance matrix of the network. The problem is constrained by the power flow in each line $\underline{P_l} \leq P_l\theta \leq \overline{P_l}$, the maximum generation $\underline{P_G} \leq P_G \leq \overline{P_G}$, as well as the imports $\underline{P_I} \leq P_I \leq \overline{P_I}$.

The constraints for the SCOPF problem are included using LODFs as in [6] and GGDFs as in [42]. For line-outage contingency i, the post-contingency line flows are given by

$$P_l^i = (1 + LODF^i) \cdot B_f\theta \tag{44}$$

and for generator outage i the post-contingency line flows are given by:

$$P_l^i = P_l + GGDF^i \cdot P_G \tag{45}$$

Connections to external areas are modeled as variable generation nodes with a capacity-band between the minimum and maximum flow across the border line. The physical limitation of the import is given by the limit on the tie-line; thus the introduction of the tie-lines adds one set of constraints. This is included twice: once as a line flow limit, and once as a generation limit of the virtual generator.

The P-SCOPF is thus formulated by changing the post-contingency line limits. Eqn. (44) is thus reformulated to give:

$$\underline{\tilde{P}_l^i} \leq P_l^i \leq \overline{\tilde{P}_l^i} \tag{46}$$

These probabilistic limits are tighter than the line limits for *fully observ.* systems, so that $\overline{\tilde{P}_l} \leq \overline{P_l}$.

The calculation of the LODFs depends on the network topology, and can thus only be calculated for internal line outages. This fact, coupled with the islanding of the border nodes, means that tie-line outages can not be fully de-centrally formulated using LODFs, as the participating TSOs do not have sufficient information about the external network. To counter this problem, the line-outage of a tie-line is modeled as a generator outage. The use of generation outages to model tie-line outages is performed also in [43]; however, there they are not used to calculate the safe transmission capacity, but rather to explicitly model the effect of the tie-line outage. The import of energy across the tie-line acts similar to a local generator; losing it will necessitate the increase of local generation to re-establish power balance, or the redistribution of tie-line flows. The calculation of these redispatch factors is a process performed for generator outages in the GGDFs, which can easily be expanded. As the formulation no longer relies on the use of the LODFs, arbitrary correction schemes can be used, for example, shifting the tie-line flows to other importing lines, or locally correcting the loss of import. Here, we locally correct the line loss, meaning that all lost import is compensated by the increase of local generation.

Termination is determined in a cooperative manner. Termination is only achieved when all areas have reached their respective termination criterion, i.e. when the change in the state variable at the border nodes is sufficiently small.

3. Benefits and Drawbacks

The benefits of this method are primarily enhanced confidentiality and low levels of information sharing. Using the method outlined, a group of TSOs can cooperatively solve the OPF problem without exchanging information about the particular topology of their grid or generation structure.

The extension provided by the weak inter-area state-coupling on the border nodes allows the use of diverse interconnections to neighboring areas, thus enabling the extension to include HVDC-lines, single point in-feeds or even HVDC grids.

In addition to the increased modeling freedom achieved, there is no longer any need for a reference node in a reference area. In previous formulations, such as [39] and [40], one area was designated to contain the reference node, and all other areas calculated their nodes relative to this area. Using the formulation presented in this paper, there is no single reference bus, meaning that no area is more important than the others.

Using the κ-factor as a price for imported power, each area can clearly calculate how much it should be paying the other areas for power. There is thus no ambiguity on the financial flows, and the cost structure can be more properly replicated.

Drawbacks of the decentralized formulation relative to the central one include increased complexity in the exchange of data and increased calculation time. Relative to previous decentralized formulations, the formulation used in this paper has decreased complexity in the exchanged data. However, the decentralized calculation leads to the introduction of an error due since external areas are not modeled. Perhaps the biggest drawback is the fact that while the N-1 security of the own system can be calculated versus outages of the internal generators, internal lines, and tie-lines, the impact of external generator outages or external line outages can not be calculated, nor can the effect of internal contingencies on external grid components be calculated. As such, the N-1 security of each grid portion can be considered, but the N-1 security of the entire grid can not be determined.

VI.D. Case-Study – Multi-Area System

1. Effect of Forecast Error Observability

Here, we compare operation costs for four different policies: OPF, SCOPF, P-SCOPF *fully observ.* and P-SCOPF *partial-error*. Fig. 12 shows the results. The comparison is performed for a high RES in-feed scenario and a low RES in-feed scenario, characterized by 100% and 10% of the in-feeds shown in Table II.

The different formulations produce different results when the wind factor is high. The P-SCOPF leads to higher costs but higher security than the SCOPF or OPF. Moreover, the P-SCOPF fully observ. is more costly than the P-SCOPF partial-error because the P-SCOPF fully observ. scenario considers the full RES in-feed forecast error within the system.

In the simulations, we assume the variance of the forecast error is 20% of the forecasted in-feed and the probability of overloading ε is 20%. This is in contrast to the SCOPF where this probability is 50%.

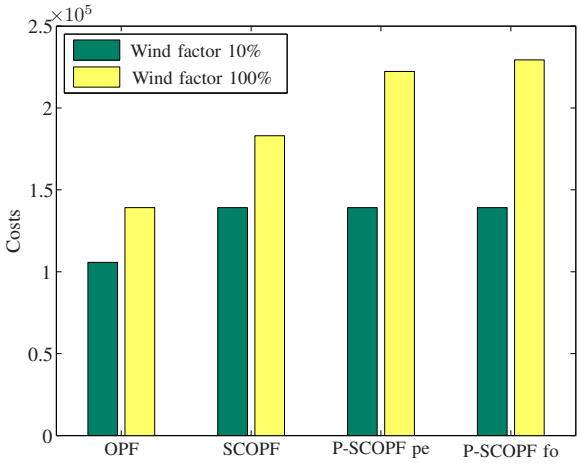

Fig. 12. Comparison between operating costs under different policies for high and low RES in-feed. 'P-SCOPF pe' refers to partial-error and 'P-SCOPF fo' refers to fully observ.

2. Results for Decentralized OPF Calculation

In this section, we investigate cases where both the topology and the RES in-feed forecast error are partially observable. We verify the decentralized OPF approach by comparing it with a well-accepted software tool.[2] For the OPF, the decentralized approach gives an RMS-error of 2.6MW (compared with a total generation of approximately 8GW). For the generation costs, the absolute difference is on the order of $2 \cdot 10^{-6}$. The results calculated with the software tool are for a single-area system while the ones for the decentralized calculation are multi-area systems.

[2]The software tool was in this case provided by matpower (R. D. Zimmerman, C. E. Murillo-Sánchez, and R. J. Thomas, "MATPOWER: Steady-State Operations, Planning and Analysis Tools for Power Systems Research and Education," Power Systems, IEEE Transactions on, vol. 26, no. 1, pp. 12-19, Feb. 2011.)

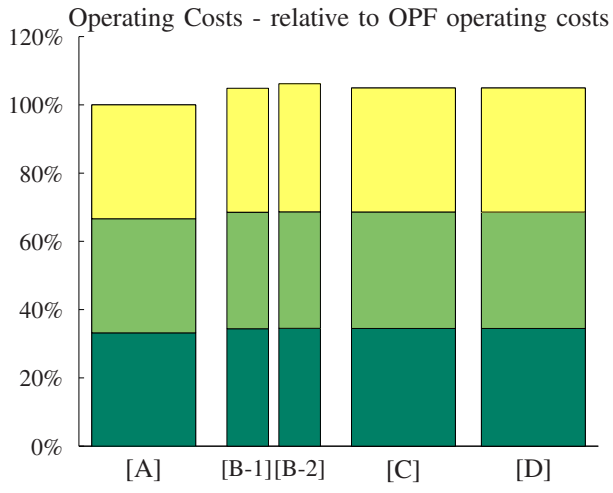

Fig. 13. Comparison between total system costs for different decentralized OPF computation schemes assuming partially observable RES in-feed forecast error (*partial observ.*), under minimal wind in-feed. Each color represents one area: dark green area 1, light green area 2, and yellow area 3. [A] is OPF, [B-1] is SCOPF with line outages, [B-2] is SCOPF with line and generation outages, [C] is P-SCOPF, and [D] is a mixed operating case using P-SCOPF in area 1 and SCOPF considering line outages in areas 2 and 3.

Figure 13 shows the comparison of costs, split between the three areas under different operating schemes. Costs are normalized to the costs of the centralized OPF without security constraints. The cases are:

- [A] the classical OPF without any security constraints
- [B-1] SCOPF, with consideration of line outages using LODF as described by (44)
- [B-2] additionally includes the treatment of generation outages as described in (45)
- [C] is a probabilistic P-SCOPF as described in Section VI-B, considering line outages, and with line limits calculated using the wind uncertainty from the area as described in III-C. The limits in this case are the ones determined by P-SCOPF partial-error from the previous subsection.
- [D] is a mixture of P-SCOPF in area 1 with line limits calculated as in [C], and SCOPF in areas 2 and 3 as in [B-1]. This mixed case shows the feasibility of using different operating schemes in different areas, without the operators having knowledge of each others scheme.

In all the security constrained cases, the generation costs are higher, as expected. As there is only minimal wind in feed (10% of the values in Table II), the influence of the probabilistic effects are not significant, as is shown by a comparison between cases [B-1] and [C]. A comparison between [B-1] and [B-2] clearly shows the importance of the generator outages.

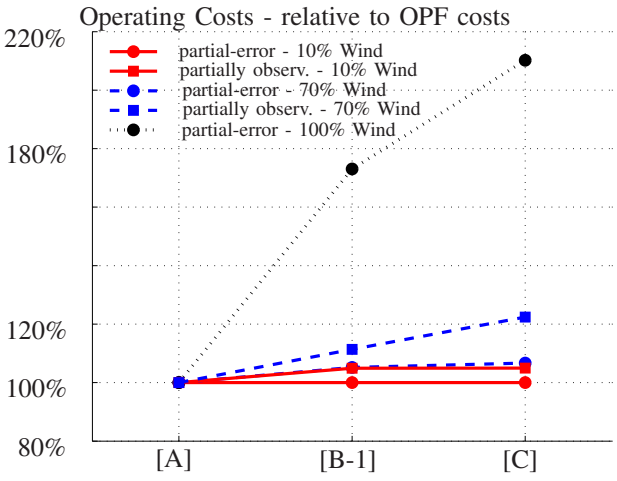

Fig. 14. Cost comparison between calculation with full observability and partial observability - The black lines indicate low wind in-feed, the blue lines indicate medium wind in-feed and the black line indicates maximum wind in-feed. Circles denote the fully observable case, and squares are the partially observable case. [A] is standard OPF without security limits, [B-1] is standard SCOPF with line outages, while [C] depicts P-SCOPF

In this case, the difference in cost is not pronounced between the SCOPF and P-SCOPF cases, as there is very little RES in-feed. This result is consistent with those in the remainder of the paper. In the following section, the influence of higher RES in-feed will be considered.

3. Effect of Topological Observability

This section combines the previous approaches to show the comparison between full and partial knowledge of grid topology. The comparison shown here is only based on the total operating costs for the entire system, there is no comparison of the cost for each area.

We again compare cases [A], [B-1] and [C]. The wind in-feed is set to 10%, 70% and 100% of values in Table II. Figure 14 presents a comparison between the total system operating costs for the system. They are normalized to the cost of operating the system under OPF without security considerations. Thus, the figure shows only the increase in system operation costs due to security limits. Generally, it can be said that increased security considerations increases the cost of system operation. This is seen by the increasing system costs, and is true for both cases.

The costs for the partially observable system are always higher than the costs for the partial-error case. One reason for the higher operating costs in the decentralized calculation is that the system considered is tightly meshed. As the system operators overestimate the post-contingency line-flows the generator dispatch is more costly. The overestimation of post-contingency line flows comes from the lack of knowledge about external areas, and can be substantial. In order to illustrate this fact, we consider the outage of the line between nodes 113 and 123. These two nodes can very roughly be thought to be connected by three paths: a direct connection, a connection inside area 1, and a connection inside area 2. The direct connection has a reactance of 0.0865p.u., the shortest parallel path on the internal side of the border has a reactance of 0.1442p.u., and the shortest parallel connection on the external side of the border has a the reactance of 0.1922p.u. As a gross approximation the power flowing across this line would be approximately equally split between the internal and external lines if the full system model were considered. As the 3 tie-lines between areas 1 and 2 make up 30% of the lines connected to the border nodes, the influence of the cross-border power flows are clearly substantial. This problem can not be solved using a fully decentralized approach as there is no possibility with which the area can learn the network model of the neighboring system; however, additional information sharing can mitigate this issue. Due to this modeling aspect, the entire additional flow which arises from a line, or generator outage is compensated in the internal area: this creates tighter constraints. These tighter constraints do not decrease the security of the area system, as the practical flows will be lower.

A second point to note is the lack of results for 100% RES in-feed in the partially observable case. There is no way in which this level of power in-feeds can be accommodated under consideration of the remaining security limits. Here, co-operation between TSOs enables an increased RES in-feed.

VII. Discussion: Transient Stability and HVDC

In the previous sections, preventive as well as corrective control actions were developed for variety of SCOPF formulations. The operating points given as a result of these approaches were validated for feasibility from a static perspective, i.e. it was shown that the post-contingency configurations are stable operating points. However, this assumption must also be verified using time-domain simulations to ensure dynamic stability, as shown in [1].

It is possible to approximate the system dynamics in an SCOPF by using more conservative security margins. However, this will lead to a solution that does not fully utilize the capabilities of the system, and this approach does not provide firm guarantees of avoiding transiently unstable solutions. This issue is especially important in systems with high penetrations of complex devices such as Flexible AC Transmission System (FACTS) and HVDC links, since their dynamics are important.

One way to address this challenge is to extend the standard SCOPF to a Transient Stability Constrained Optimal Power Flow (TSCOPF). In a TSCOPF, the system dynamics are included as algebraic equations or inequalities, as proposed in [44]. However, adding these stability constraints transforms the problem into a complex nonlinear program, and high computational effort is needed to solve such a problem.

In general, VSC-HVDC links improve the controllability of the

system. The stability of a system can be improved by dynamically changing the set points of the VSC-HVDC link during transients. In particular, we can control the active and reactive power that the converters withdraw from, or inject into, the grid. This allows us to use VSC-HVDC for voltage stability control and power oscillation damping. The authors in [45] propose using VSC-HVDC to guarantee that the generators will not lose synchronism. In [46], the authors show that using Model Predictive Control (MPC) to determine the control trajectory significantly improves damping during transients. The effect is achieved by simultaneously manipulating the set points of several installed VSC-HVDC links in a large system.

While VSC-HVDC has the potential to improve the controllability of the system, the full advantages of this technology can only be realized by adequately considering the system dynamics. Finding suitable simplifications for the system dynamics – analogous to DC power flow approximations – remains an open question.

VIII. Conclusions

This paper presents a variety of different SCOPF formulations addressing four power system operation and planning problems: (a) forecast uncertainty of RES in-feed and load, (b) security criteria based on contingency risk, (c) corrective control offered through HVDC lines and flexible demand, and (d) operation of multi-area systems with limited data exchange.

Starting from a deterministic SCOPF with the "standard" N-1 criterion, the formulation is extended step-wise to a probabilistic SCOPF taking into account load and wind forecast errors, corrective control actions of VSC-HVDC lines and flexible demand, and a risk-based security criterion. In addition to VSC-HVDC PTP links, MTDC grids are also investigated. Subsequently, a distributed SCOPF algorithm is introduced, where each TSO is responsible for its own control area and receives limited information from neighboring areas. We distinguish between two types of limited observability for the neighboring areas: (i) limited information on RES forecast errors, and (ii) limited information of the grid topology.

Our contributions include 1) a comprehensive probabilistic SCOPF framework based on scenario-based methodologies, where different levels of uncertainty, controllability, and contingency risk are incorporated in one algorithm, 2) a distributed probabilistic SCOPF algorithm for multi-area systems, and 3) an analysis of the performance of the different SCOPF formulations on the three-area RTS-96 system.

The case studies results lead to the following conclusions:

- Incorporating load and wind forecast error uncertainty in the day-ahead operation planning can significantly increase the costs of generation dispatch (up to 10% in our case study).
- Corrective control actions offered through HVDC lines and flexible demand can counter the effects of uncertainty and limit the increase in operating costs (up to 50% in our case study).
- Corrective control actions of HVDC lines allow a higher integration of wind generation and can postpone or avoid investments in new AC lines.
- Point-to-Point HVDC links lead to lower operating costs and higher wind power penetration than Multi-Terminal HVDC grids or an equal number of AC lines. However, the investment costs for building PTP links are substantially higher than connecting the lines in a meshed MTDC grid.
- Knowledge of wind forecast errors of neighboring areas tightens the line constraints in the area in question, leading to higher operating costs.
- Limited knowledge of the grid topology of neighboring areas leads to higher operating costs. This occurs because the area in question assumes that, in the case of a contingency, neighboring areas cannot accommodate any of the resulting flows. The assumption that all post-contingency flows are contained within the same area leads to the tightening of the line flow constraints, and thus to higher operating costs. This effect becomes more evident with higher shares of wind power integration. This highlights the need for close cooperation among individual TSOs.

Acknowledgements

Research was supported by the European Commission under the projects IRENE-40, FP7-TREN-218903 and Umbrella, 282775-2. We further acknowledge the support for the projects "Multi-Area Security (MARS)" (swisselectric research), "Power System Performance Enhancement by Use of Voltage Source Converter Based HVDC in the ENTSO-E RG Continental Europe System" (swisselectric research and ABB) and "HVDC networks" (ABB, Alstom, Siemens and the Swiss Federal Office of Energy).

References

[1] F. Capitanescu, J.L. Martinez Ramos, P. Panciatici, D. Kirschen, A. Marano Marcolini, L. Platbrood, and L. Wehenkel. State-of-the-art, challenges, and future trends in security constrained optimal power flow. *Electric Power Systems Research*, 81(8):1731 – 1741, 2011.

[2] O. Alsac and B. Stott. Optimal load flow with steady-state security. *IEEE Transactions on Power Apparatus and Systems*, PAS-93(3):745–751, 1974.

[3] A. Monticelli, M. V F Pereira, and S. Granville. Security-constrained optimal power flow with post-contingency corrective rescheduling. *IEEE Transactions on Power Systems*, 2(1):175–180, 1987.

[4] M. Vrakopoulou, K. Margellos, J. Lygeros, and G. Andersson. Probabilistic guarantees for the n-1 security of systems with wind power generation. *Proceeding of Probabilistic Methods Applied to Power Systems Conference*, pages 858–863, 2012.

[5] T. Krause. *Evaluating Congestion Management Schemes in Liberalized Electricity Markets Applying Agent-based Computational Economics*. PhD thesis, ETH Zurich, Switzerland, 2007.

[6] R.D. Christie, B.F. Wollenberg, and I. Wangensteen. Transmission management in the deregulated environment. *Proceedings of the IEEE*, 88(2):170 –195, February 2000.

[7] W.Y. Ng. Generalized generation distribution factors for power system security evaluations. *IEEE Transactions on Power Apparatus and Systems*, PAS-100(3):1001 –1005, 1981.

[8] S. Chatzivasileiadis, T. Krause, and G. Andersson. HVDC line placement for maximizing social welfare – an analytical approach. In *IEEE PowerTech Conference*, Grenoble, France, 2013.

[9] M. Vrakopoulou, S. Chatzivasileiadis, and G. Andersson. Probabilistic security-constrained optimal power flow including the controllability of HVDC lines. In *submitted to IEEE Innovative Smartgrid Technologies (ISGT) Europe 2013*, pages 1 –6, October 2013.

[10] F. Bouffard, F.D. Galiana, and A.J. Conejo. Market-clearing with stochastic security- part i: Formulation. *IEEE Transactions on Power Systems*, 20(4):1818 – 1826, 2005.

[11] F. Bouffard, F.D. Galiana, and A.J. Conejo. Market-clearing with stochastic security- part II: Case Studies. *IEEE Transactions on Power Systems*, 20(4):1818 – 1826, 2005.

[12] F. Bouffard and F.D. Galiana. Stochastic security for operations planning with significant wind power generation. *IEEE Transactions on Power Systems*, 23(2):306 – 316, 2008.

[13] K. Hedman, M. Ferris, R.P. O'Neill, E. Bartholomew, and S. Oren. Co-optimization of generation uinit commitment and transmission switching with n-1 reliability. *IEEE Transactions on Power Systems*, 25(2):1052–1063, 2010.

[14] L. Roald, F. Oldewurtel, T. Krause, and G. Andersson. Analytical reformulation of security constrained optimal power flow with probabilistic constraints. In *IEEE PowerTech Conference*, Grenoble, France, 2013.

[15] S. Boyd and L. Vandenberghe. Convex Optimization. *Cambridge University Press*, 2004.

[16] O. Mäkelä and G. Andersson. Propagation of power flows from wind power in neighboring control areas in multi-area power systems. In *IEEE PowerTech Conference*, Grenoble, France, 2013.

[17] G. Calafiore and M. Campi. The scenario approach to robust control design. *IEEE Transactions on Automatic Control*, 51(5):742–753, 2006.

[18] K. Margellos, P. Goulart, and J. Lygeros. On the road between robust optimization and the scenario approach for chance constrained optimization problems. *submitted to IEEE Transactions on Automatic Control*, 2012.

[19] M. Vrakopoulou, K. Margellos, J. Lygeros, and G. Andersson. A Probabilistic Framework for Reserve Scheduling and N-1 Security Assessment of Systems with High Wind Power Penetration. *submitted to IEEE Transactions on Power Systems*, 2012.

[20] M. Vrakopoulou, K. Margellos, J. Lygeros, and G. Andersson. A Probabilistic Framework for Security Constrained Reserve Scheduling of Networks with Wind Power Generation. *IEEE International Conference & Exhibition (ENERGYCON)*, pages 508–513, 2012.

[21] M. Vrakopoulou, M. Katsampani, K. Margellos, J. Lygeros, and G. Andersson. Probabilistic security-constrained AC optimal power flow. In *IEEE PowerTech Conference*, Grenoble, France, 2013.

[22] T. Alamo, R. Tempo, and A. Luque. On the sample complexity of randomized approaches to the analysis and design under uncertainty. *American Control Conference*, pages 4671 – 4676, 2010.

[23] D. Bertsimas and M. Sim. Tractable Approximations to Robust Conic Optimization Problems. *Mathematical Programming, Series B*, 107:5–36, 2006.

[24] W. Fu and J. D. McCalley. Risk-based optimal power flow. In *IEEE PowerTech Conference*, Porto, Portugal, 2001.

[25] F. Xiao and J. D. McCalley. Power system assessment and control in a multi-objective framework. *IEEE Trans. Power Syst.*, 24:78–85, 2009.

[26] Q. Wang and J. D. McCalley. A computational strategy to solve preventive risk-based security constrained OPF. 2012.

[27] F. Oldewurtel L. Roald, M. Vrakopoulou and G. Andersson. Risk-constrained optimal power flow with probabilistic guarantees. In *submitted to IEEE ISGT Conference*, Copenhagen, Denmark, 2013.

[28] J.L. Mathieu, M. Kamgarpour, J. Lygeros, and D.S. Callaway. Energy arbitrage with thermostatically controlled loads. In *Proceedings of the European Control Conference*, Zürich, Switzerland, 2013.

[29] J.L. Mathieu, M. González Vayá, and G. Andersson. Uncertainty in the flexibility of aggregations of demand response resources. In *In review for IECON*, Vienna, Austria, 2013.

[30] R. Wiget and G. Andersson. Optimal power flow for combined AC and multi-terminal HVDC grids based on VSC converters. In *Power and Energy Society General Meeting, 2012 IEEE*, pages 1–8, 2012.

[31] S. Chatzivasileiadis, T. Krause, and G. Andersson. Security-constrained optimal power flow including post-contingency control of VSC-HVDC lines. In *XII SEPOPE, Rio de Janeiro, Brazil*, pages 1 –12, May 2012.

[32] J. Sun and L. S. Tesfatsion. DC optimal power flow formulation and solution using QuadProg. *Economics Department, Iowa State University*, 6014:1–36, 2006.

[33] R. Wiget and G. Andersson. DC optimal power flow including HVDC grids. In *Electrical Power and Energy Conference (EPEC 2013)*, pages 1–6, 2013.

[34] C. Grigg, P. Wong, P. Albrecht, R. Allan, M. Bhavaraju, R. Billinton, Q. Chen, C. Fong, S. Haddad, S. Kuruganty, W. Li, R. Mukerji, D. Patton, N. Rau, D. Reppen, A. Schneider, M. Shahidehpour, and C. Singh. The ieee reliability test system-1996. a report prepared by the reliability test system task force of the application of probability methods subcommittee. *IEEE Transactions on Power Systems*, 14(3):1010–1020, 1999.

[35] G. Papaefthymiou and B. Klöckli. MCMC for wind power simulation. *IEEE Transactions on Energy Conversion*, 23(1):234–240, 2008.

[36] P.W. Sauer. On the formulation of power distribution factors for linear load flow methods. *Power Apparatus and Systems, IEEE Transactions on*, PAS-100(2):764 –770, feb. 1981.

[37] J.F. Dopazo, O.A. Klitin, and A.M. Sasson. Stochastic load flows. *Power Apparatus and Systems, IEEE Transactions on*, 94:299–309, 1975.

[38] P.N. Biskas and A.G. Bakirtzis. A decentralized solution to the security constrained DC-OPF problem of multi-area power systems. In *Power Tech, 2005 IEEE Russia*, pages 1–7, 2005.

[39] A.J. Conejo and J.A. Aguado. Multi-area coordinated decentralized DC optimal power flow. *Power Systems, IEEE Transactions on*, 13(4):1272–1278, 1998.

[40] P.N. Biskas and A.G. Bakirtzis. Decentralised opf of large multi-area power systems. *Generation, Transmission and Distribution, IEE Proceedings-*, 153(1):99–105, 2006.

[41] E. Iggland and G. Andersson. On using reduced networks for distributed DC power flow. In *Power and Energy Society General Meeting, 2012 IEEE*, pages 1–6, 2012.

[42] P.N. Biskas and A.G. Bakirtzis. Decentralised security constrained DC-OPF of interconnected power systems. *IEE Proceedings-Generation, Transmission and Distribution*, 151(6):747 – 754, 2004.

[43] J.-H. Kim, J.-K. Park, B.H. Kim, J.-B. Park, and D. Hur. A method of inclusion of security constraints with distributed optimal power flow. *International Journal of Electrical Power & Energy Systems*, 23:pp.189–194, 2001.

[44] D. Gan, R.J. Thomas, and R.D. Zimmerman. Stability-constrained optimal power flow. *Power Systems, IEEE Transactions on*, 15(2):535–540, 2000.

[45] S. Chatzivasileiadis, D. Ernst, and G. Andersson. The global grid. *Renewable Energy*, 57(0):372 – 383, 2013.

[46] A. Fuchs, M. Imhof, T. Demiray, and M. Morari. Stabilization of large power systems using VSC-HVDC and model predictive control. *submitted to IEEE Transactions on Power Delivery - Special Issue on HVDC Systems and Technology*, 2013.